IEEE Access
Multidisciplinary : Rapid Review : Open Access Journal

Received September 29, 2018, accepted October 9, 2018, date of publication October 12, 2018, date of current version November 8, 2018.

*Digital Object Identifier 10.1109/ACCESS.2018.2875723*

# Lightning Transient Analysis of Telecommunication System With a Tubular Tower

**HONGCAI CHEN[1], (Member, IEEE), YANG ZHANG[2], YAPING DU[2], AND QINGSHA S. CHENG[3], (Senior Member, IEEE)**
[1]SUSTech Academy for Advanced Interdisciplinary Studies, Southern University of Science and Technology, Shenzhen 518055, China
[2]Department of Building Service Engineering, The Hong Kong Polytechnic University, Hong Kong
[3]Department of Electrical and Electronic Engineering, Southern University of Science and Technology, Shenzhen 518055, China

Corresponding authors: Yang Zhang (16103271g@connect.polyu.hk) and Qingsha S. Cheng (chengqs@sustc.edu.cn)

This work was supported in part by the National Natural Science Foundation of China under Grant 61471258, in part by the Science and Technology Innovation Committee of Shenzhen Municipality under Grant KQJSCX20170328153625183, and in part by the Research Grants Council of HKSAR under Grant 152038/15E.

**ABSTRACT** Unexpected lightning strikes on telecommunication towers may damage sophisticated communication equipment. Thus, it is necessary to predict transient currents in the telecommunication system (TS). Modeling the TS with the tubular tower is an essential but complex work. This paper presents a modeling procedure for the TS with the tubular tower. An efficient meshing scheme is proposed to model a system composed by conductors with both large and small radii. Both skin and proximity effect as well as propagation effect are considered using a partial element equivalent circuit method. The time-domain solution is finally obtained using the extended equivalent circuit. The procedure is verified through numerical comparison. The transient currents in the TS with a 40-m tubular tower are finally analyzed. The simulation shows that more currents will flow in outer-located conductors than other conductors. Particularly, more currents dissipate through the earth bus far from the lightning strike. It provides principles to design effective lightning protection and select appropriate protective devices for TS.

**INDEX TERMS** Lightning protection, telecommunication system, radio base station, tubular tower, transient analysis.

## I. INTRODUCTION

Recent progress in telecommunication technology has led to the development of complex telecommunication systems (TSs). With the increasing customer's demand, the reliability of TSs is essential for communication service providers. Telecommunication facilities contain many vulnerable low-voltage electronic devices. These devices could be easily destroyed by surges arising from by a lightning current of several kilo amperes. Reported lightning-related accidents on TSs [1] have drawn an increasing attention from both industry and academy.

To study the effectiveness of lightning protection modules, transient currents in a TS need to be assessed. Experiments can reveal lightning transient currents in a TS directly. Tominaga *et al.* [2] observed transient currents in a practical TS under natural lightning. Barbosa *et al.* [3] and Dai *et al.* [4] presented their measured results in TSs obtained under rocket-triggered lightning. Note that it is both time consuming and costly as it is difficult to perform experimental tests for every possible change or configuration of the system.

An efficient way of evaluating a TS is the computer simulation. Numerical methods based on the circuit theory and electromagnetic theory such as finite-difference time-domain (FDTD) method [5]–[8], partial element equivalent circuit (PEEC) method [9]–[13], etc. have been proposed for transient analysis. Grcev *et al.* [14] studied surges in TSs mounted on power transmission lines using method of moment (MoM). Modeling of the buried conductor network consisting of connected grounding electrodes and power cables were presented. The transient current distribution and overvoltages in the power cables and the grounding system was analyzed. While, the tower and signal cables were not investigated. Mikropoulos *et al.* [15] investigated the overvoltages impinging on the distribution transformer due to direct lightning strokes to the nearby TS tower using ATP-EMTP simulations. It is noted that only the cables were simulated to address the failure of the distribution transformer. Steel towers and signal cables in TS were not included in the model. Tatematsu *et al.* [16] analyzed the lightning current distribution in a TS with a steel tower using FDTD method. An experiment on a reduced-scale TS was also provided to verify the calculation results. Although the steel tower, grounding grid and cables were considered in the simulation, SPDs were not included. Chen *et al.* [17] and Chen and Du [18] presented a partial element equivalent circuit (PEEC) based method for calculating lightning transient currents in a TS. The system was mounted on a steel tower. Laboratory tests on a simplified TS were performed for validating the method. Several issues including ferromagnetic steels, proximity effect among cables, nonlinear SPDs, grounding grid etc. were addressed in the simulation.

These studies, however, focus on the system mounted on steel towers or lattice steel structures. Little work has been reported on the transient analysis of a TS mounted on a tubular tower. Recently tubular towers become more and more popular due to landscape design, flexible installation, and less construction land. A tubular tower is the hollow, columnar metal structure with a radius of dozens cm and a thickness of approximate 10 mm. When modeling tubular tower system, both skin and proximity effects among tower and cables need to be addressed appropriately. Meanwhile, protective devices and electronic components in the TS should be also included in the system analysis.

In this paper, a comprehensive modeling method for different components in the TS mounted on a tubular tower is presented. Modelling of the tubular tower, cables and the eddy current effect between them is introduced. Section II briefly describes a PEEC based method for impedance extraction of the tower and cables. The eddy current effect between the tower and cables is investigated numerically and modeling guidelines are summarized. Section III introduces other components used in the TS, including surge protective devices (SPDs), grounding grids, etc. Experiments on individual tubular structures, and current sharing among the tubular structure and copper wires are presented in Section IV for verifying the proposed method. Finally, transient current distribution in a practical TS is simulated.

## II. SYSTEM MODELLING AND SIMULATION METHODOLOGY

The partial element equivalent circuit (PEEC) method is adopted as fundamental tool to solve electromagnetic effects in the tubular system. The PEEC method [19] has been developed to transform the problem in the electromagnetic domain to the circuit domain. This method originates from the integral form of Maxwell's equations, and represent the electromagnetic fields using lumped circuit elements. Rewriting the Maxwell's equations in the vector potential form, the electric field is expressed by a magnetic vector potential $\boldsymbol{A}$ and an electric scalar potential $\varphi$ as

$$\boldsymbol{E}^i = \frac{\boldsymbol{J}(\boldsymbol{r})}{\sigma} + j\omega \boldsymbol{A}(\boldsymbol{r}) + \nabla\phi(\boldsymbol{r}) \tag{1}$$

where $\boldsymbol{E}^i$ is the incident field, $\boldsymbol{J}$ is the current density at a source point, $\boldsymbol{r}$ is the location of the source point, $\sigma$ is the electric conductivity of the conductor, and $\omega$ is the angular frequency of the current. Both vector $\boldsymbol{A}$ and scalar potentials $\varphi$ can be expressed using the Green's function. In our formulation, free space Green's function is adopted where the retardation term is neglected. That is reasonable assumption because the tower is short compared to the wavelength. The wavelength in the air at 1 MHz is 300m. A 40 m tower is less than 1/7 of the wavelength. Therefore, the retardation term can be neglected in the calculation. With the assumption of constant current density and charge density in each PEEC cell, partial element parameters: resistance $\boldsymbol{R}$, inductance $\boldsymbol{L}$ and coefficient of potential $\boldsymbol{P}$ are obtained, as listed in Table 1. Coefficients of potential (CoP) cannot be used in circuit solvers directly. While, it can be transformed into the capacitance using the relation in the matrix form as $\boldsymbol{C} = \boldsymbol{P}^{-1}$.

Lightning transient current has a fast wavefront that the propagation effect is significant along a long line. In order to consider the propagation of lightning current, the length of the segment is determined with the following criterion [20]

$$\Delta l < \frac{1}{10}\frac{c}{f_m} \tag{2}$$

where $c$ is the velocity of light and $f_m$ is the maximum frequency of concern.

The lightning current travels along the tower to the ground when the tower is stroked by lightning. Note that lightning transient current has a wide frequency range. Accurate calculation of partial elements requires considering skin and proximity effects [21], [22]. A tubular tower takes the shape of the hollow truncated cone as shown in Fig. 1. In this paper, the tower as well as the cable mounted on the tower is discretized into a certain number of segments with the length being determined by (2). Each segment of the tower is approximately taken as a hollow cylinder. The cable segments are similar to the tower segment, except that their cross-section dimensions are much less. Fig. 1 illustrated the configuration of the tubular system and its equivalent circuit obtained using the PEEC method. Both $Z_1$ and $Z_2$ represent the cable and tower impedance, respectively. $C_{ij}$ represents capacitance between cable and tower segments or capacitance to the ground. Mutual inductance and mutual capacitance between unaligned segments also exist. For simple illustration, these components are not shown in the figure.

Note that both current and charge densities are unevenly distributed on the cross section of segments, because of skin and proximity effects. The formulas given in Table 1 are then not applicable to those parameters presented in Fig. 1. Volume or surface meshing techniques are applied in order to find out equivalent circuit parameters of segments. For unaligned segments, the influence of skin and proximity

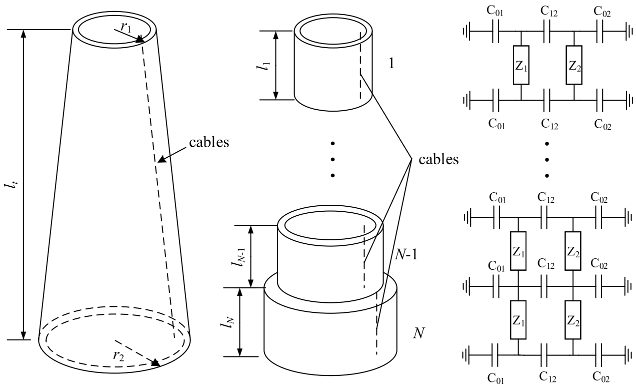


**FIGURE 1. Discretization of the tubular tower and the cable in the lengthwise direction.**

**TABLE 1. Expressions for partial elements.**

| Partial Element Type | Partial Element Expression |
|---|---|
| Resistance | $R_i = \dfrac{l_i}{\sigma_i a_i}$ |
| Partial inductance | $L_{ij} = \dfrac{\mu_0}{4\pi}\dfrac{1}{a_i a_j}\int_{V_i}\int_{V_j}\dfrac{1}{\lvert \mathbf{r} - \mathbf{r}' \rvert} dV_i dV_j$ |
| Coefficients of potential | $P_{ij} = \dfrac{1}{4\pi\varepsilon}\dfrac{1}{S_i S_j}\int_{S_i}\int_{S_j}\dfrac{1}{\lvert \mathbf{r} - \mathbf{r}' \rvert} dS_i dS_j$ |

* $\mathbf{r}'$ is the position of the observation point, $a$ is the area of the cross section of the conductor and $S$ is the area of the surface of the conductor.

effects is not significant, a simplified procedure is proposed to calculate mutual inductance and coefficient of potential. The detail is given in Appendix. The circuit parameters for aligned segments are discussed in the following sections.

### *A. PARTIAL IMPEDANCE OF ALIGNED SEGMENTS*

A volume filament model [12], [23] is adopted to calculate frequency-dependent impedance for aligned parallel segments. To cater for uneven current distribution in segments, each of them is divided into parallel filaments with constant current density on their cross section. Frequency-dependent impedance is then obtained by solving the circuit network representing the coupled filaments.

Because of large dimensions of the tower, a significant number of meshing elements are required for modeling. To improve the efficiency of segment modeling, a non-uniform meshing scheme is employed to mesh the cross section of each segment. In this scheme the tubular tower is divided into a single layer of annular sectors with different sizes, as seen in Fig. 2. Fig. 2 shows respectively the mesh configurations for both tubular segment and cable segments, which are highlighted in grey color. An adaptive meshing technique is adopted for tower segments which allows denser meshing at the location near cables. The meshing is determined in a Gaussian function's style as follows

$$s = \sum_{i=1}^{N_f} \frac{1}{\underline{\sigma}\sqrt{2\pi}} e^{-\frac{\varphi-\theta_i}{2\underline{\sigma}^2}} \Big/ N_f + \frac{1}{5} \tag{3}$$

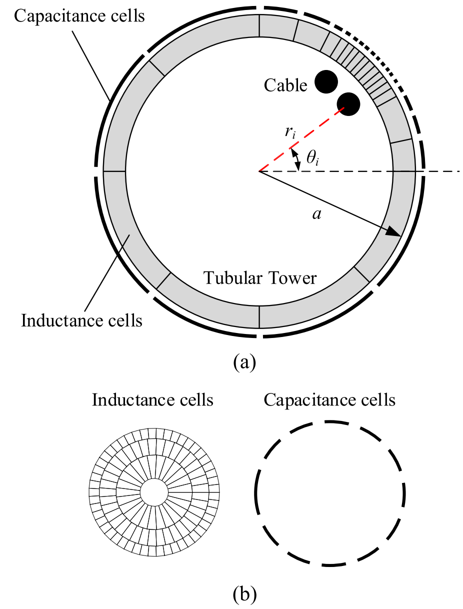


**FIGURE 2. Discretization on the cross section of conductors for capacitance cell. (a) Nonuniform meshing scheme for tubular tower. (b) Nonuniform meshing schemem for cables.**

where $N_f$ is the number of the cable, $\theta_i$ is the rotation angle of the cable to the center of the tower, $\underline{\sigma}$ is a constant which is set to be 0.1, and $\varphi$ is the angle from 0 to $2\pi$. $s$ will be used in the further step.

The result of $s$ is a superposition of several Gaussian functions as displayed in Fig. 3. The meshing is finally obtained by an iteration process to divide the angles based on the equal area rule as indicated by $S_m = S_n$.

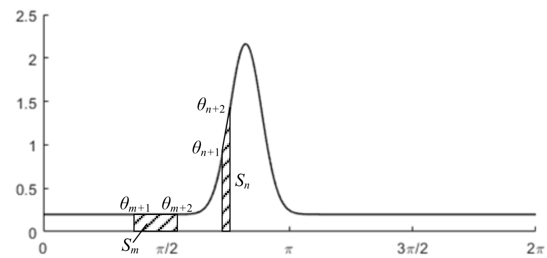


**FIGURE 3. The curve of *s* when two groups of cables are installed in the tower. The shielded areas represent two equal areas.**

The cables are installed in the tubular tower and they are closely spaced. Thus, proximity effect among these cables is significant so that denser meshing is required. The cross section of cables is discretized into several layers of annular sectors [12], [22], as shown in Fig. 2(b). The discretization in the radial direction is determined by the following expression where represent a 10% exponentially decrease at each layer as

$$dr = \ln(x) \cdot \delta \tag{4}$$

where $dr$ is the radial indent length, $x = 90\%, 80\%, \ldots, 10\%, 1\%, 0.1\%$.

The number of cells $N_a$ in the azimuthal direction is determined with an empirical formula related to the skin depth as

$$N_a = 3.52 \cdot \left(\delta/a\right)^{-0.7} + 4.35 \tag{5}$$

where $a$ is the outer radius of the conductor.

As current density in each filament is constant, inductance of each filament can be obtained directly using the volume integral as described in Appendix II. By adding the dc resistance of each filament, a matrix equation with $N$ filaments for aligned segments can be represented using parallel connected RL branches [12], [23], and is given by

$$V_s \cdot \begin{bmatrix} 1 \\ 1 \\ \vdots \\ 1 \end{bmatrix} = \begin{bmatrix} R_1+sL_{11} & sL_{12} & & sL_{1N} \\ sL_{21} & R_2+sL_{22} & \cdots & sL_{2N} \\ & \vdots & \ddots & \\ sL_{N1} & sL_{N2} & & R_N+sL_{NN} \end{bmatrix} \cdot \begin{bmatrix} I_1 \\ I_2 \\ \vdots \\ I_N \end{bmatrix} = \boldsymbol{Z}_s \cdot \boldsymbol{I} \tag{6}$$

Impedance of conductors in a segment can then be obtained by solving the parallel RL coupled circuit network, as follows:

$$\boldsymbol{Z}_c = \left[\boldsymbol{B} \cdot \boldsymbol{Z}_s^{-1} \cdot \boldsymbol{B}^T\right]^{-1} \tag{7}$$

where $\boldsymbol{Z}_c$ is the $M \times M$ impedance matrix of aligned parallel segments, $\boldsymbol{Z}_s$ is the $N \times N$ impedance matrix of the filaments given in (6). In (6) $M$ is the number of segments, $N$ is the number of filaments, and $\boldsymbol{B}$ is the selection matrix with the dimension of $M \times N$. $\boldsymbol{B}$ is composed by ones and zeros where the element $\boldsymbol{B}(k, j)$ is 1 if the $j$th cell belongs to the $k$th segment.

### B. PARTIAL CAPACITANCE OF ALIGNED SEGMENTS

Note that electric charge is situated on the surface of segments. Similar to the calculation of the inductance, a non-uniform surface meshing scheme is employed for segments in order to cater for uneven distribution of charge on the surface. Now the segment is discretized into a number of arc-shell elements with zero thickness, as illustrated in Fig. 2. The meshing size is determined with the same procedure presented in (3). The CoP is obtained using arc shell integral for parallel aligned conductors as described in Appendix IV. The matrix equation for the potential of elements in aligned segments is given by

$$V_s \cdot \begin{bmatrix} 1 \\ 1 \\ \vdots \\ 1 \end{bmatrix} = s \begin{bmatrix} p_{11} & p_{12} & & p_{1N} \\ p_{21} & p_{22} & \cdots & p_{2N} \\ & \vdots & \ddots & \\ p_{N1} & p_{N2} & & p_{NN} \end{bmatrix} \cdot \begin{bmatrix} q_1 \\ q_2 \\ \vdots \\ q_N \end{bmatrix} = s\boldsymbol{P}_s \cdot \boldsymbol{q} \tag{8}$$

CoP of elements in a segment can also be calculated using (7) by replacing $\boldsymbol{Z}_s$ with $\boldsymbol{P}_s$. Finally, CoP is transformed to the partial capacitance using $C = P^{-1}$. The partial capacitance can be finally integrated into circuit solver directly.

### C. EQUIVALENT CIRCUIT

Partial capacitance is frequency independent so that it can be implemented in the circuit solver directly. While, the partial impedance cannot due to its frequency dependence. A Vector Fitting technique (VF) [24] has to be adopted to generate the equivalent circuit by providing rational approximation of the impedance.

The impedance is approximated with rational functions based on the calculation at sampled frequencies as

$$Z_i\left(s\right) = R_i + sL_i + \sum_{m=1}^{N} \frac{s}{s - p_m} R_m \tag{9}$$

where $R_i$ and $L_i$ equal to DC resistance and the inductance of the conductor, terms with poles represent the frequency dependent effects. The resulting rational function can be implemented with RL circuits [25].

Fig. 4 shows a representative equivalent circuit of proposed method. The equivalent circuit for frequency dependent partial impedance is between the nodes $i$ and $j$. The RL parallel pairs is generated by the VF to include the frequency dependent effect. $R_i$ and $L_i$ equals to DC resistance and inductance of segments, and $L_{ij}$ represents the mutual partial inductance between segments. $C_i$ and $C_j$ denotes the partial capacitance to each node, and $C_{i,j}$ is the mutual partial capacitance between the surface elements.

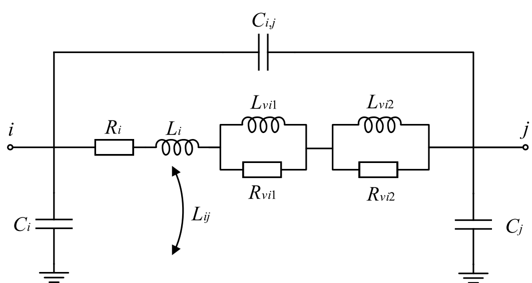


**FIGURE 4.** Equivalent circuit for VF enhenced PEEC branch.

## III. NUMERICAL VALIDATION

In order to validate the proposed method, numerical validations are presented. Firstly, calculation of the same tubular conductor using one and two segments is presented to verify the calculation of unaligned conductors using semi-analytical formulas in the Appendices. Secondly, a tower system with three coaxial cables is calculated using commercial solver to verify the efficiency of the proposed meshing scheme on the cross section.

### A. VALIDATION OF THE UNALIGNED CONDUCTOR CALCULATION

The mutual couplings between unaligned conductors are calculated using semi-analytical formulas as shown in Appendix. The validation of the unaligned conductor calculation is based on the assumption that calculated total impedance of a tubular conductor should be the same using

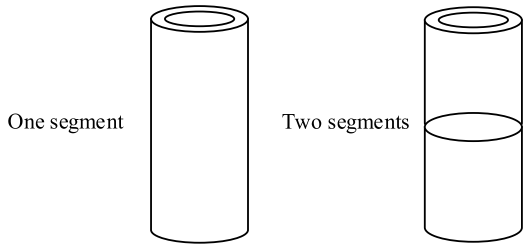


**FIGURE 5.** Configuration of numerical validation for the unaligned conductors.

one- or two- segments. As the self-impedance of a cylinder can be solved analytically, the semi-analytical formulas can be validated if the total impedance of one- and two- segments is the same.

The self-impedance is calculated for both one- and two-segment cases using the analytical formula [26]. The mutual inductance for two segment case is calculated using cylindrical shell-filament integral formulas (12). Consequently, the total inductance $L_T$ for two- segment case should obtained by $L_T = 2 \times (L_s + L_m)$ based on the circuit connection, where $L_s$ and $L_m$ are self- and mutual- inductance for two- segment case. The tubular section with radius of 500 mm, thickness of 8 mm, and length of 15 m, is evaluated and the total inductance is listed in Table 2. The one- and two- segment cases match well, which verifies the proposed method. It is also revealed that the mutual inductance between unaligned conductors varies slightly with the frequency.

**TABLE 2.** Inductance comparison between one- and two- segment cases.

| f (Hz) | Segment | 100 | 1k | 10k | 100k | 1000k |
|---|---|---|---|---|---|---|
| | One- | 9.383 | 9.383 | 9.379 | 9.371 | 9.368 |
| L (μΩ) | Two- | 9.383 | 9.383 | 9.379 | 9.371 | 9.368 |
| | Error(%) | 0 | 0 | 0 | 0 | 0 |

### B. VALIDATION OF MESHING SCHEME

The proposed meshing scheme has been validated numerically with a conductor system consisting of a tubular tower with three cables as shown in Fig. 6. Three adjacent coaxial cables are installed in a tubular tower and are located close to the surface of the tower. The tower, made of steel ($u_r = 60$, $\sigma = 1.5 \times 10^6$), has a radius of 500 mm and thickness of 8 mm. The coaxial cable, made of copper ($\sigma = 5.8 \times 10^7$ S/m), has a sheath with a radius of 12.45 mm and thickness of 1 mm, and a core with a radius of 5 mm.

Note that 3D calculation of circuit parameters of a tubular tower is difficult to perform with commercial software. A very long tower with the length of 100 m is selected so that the influence of fringe effects can be neglected and comparison can be made by using a 2D commercial solver.

Impedance of both the tower and cables are calculated with (a) the proposed 3D method and (b) a 2D BEM solver OERSTED [27]. Fig. 7 shows resistance, self- inductance and mutual inductance of the tower in the frequency range from

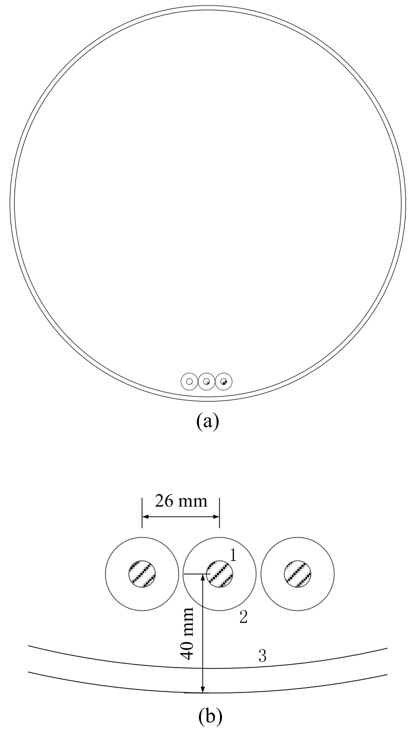


**FIGURE 6.** Configuration of a test system with 3 cables installed in a tower. Index 1, 2 and 3 indicates the core and sheath of the center coaxial cable and tower, respectively.

10 Hz to 1 MHz. The parameters obtained by two methods match very well. The average error is 0.8%. This indicates correct circuit parameters can be calculated with the proposed PEEC method. The magnetic field distribution on the cross section of the test system at 10 kHz is also demonstrated in Fig. 8. It reveals that the tubular tower has great influence on the current distribution of cables within it under direct lighting strikes though it is a Faraday cage.

## IV. SYSTEM SIMULATION AND ANALYSIS

Lightning surges in a practical TS mounted on the tubular tower is investigated in this section. The system consists of the tower, cables, equipment room and grounding grid as shown in Fig. 9. A lightning air-terminal of 5 m long is installed on the top of the tower. The tower is 40 m tall with the radius of 600 mm at the bottom and 200 mm at the top. Three coaxial (COX) cables and a shielded DC (SDC) cable are assembled within the tower from the tower top to a cable ladder at the 2.5 m height above the ground as shown in Fig. 9(a). These cables are shorted connected to the tower on the top of the tower. On the bottom of the tower, the cables are prolonged to the equipment room 6 m away from the tower to connect to telecommunication facilities. The cable sheaths are grounded before and after entering the equipment room. It firstly grounded to the earthing busbar ① before entering the room. Then these cables are connected to the telecommunication facilities in the room through protection block as displayed in Fig. 9(c). Cable cores are connected

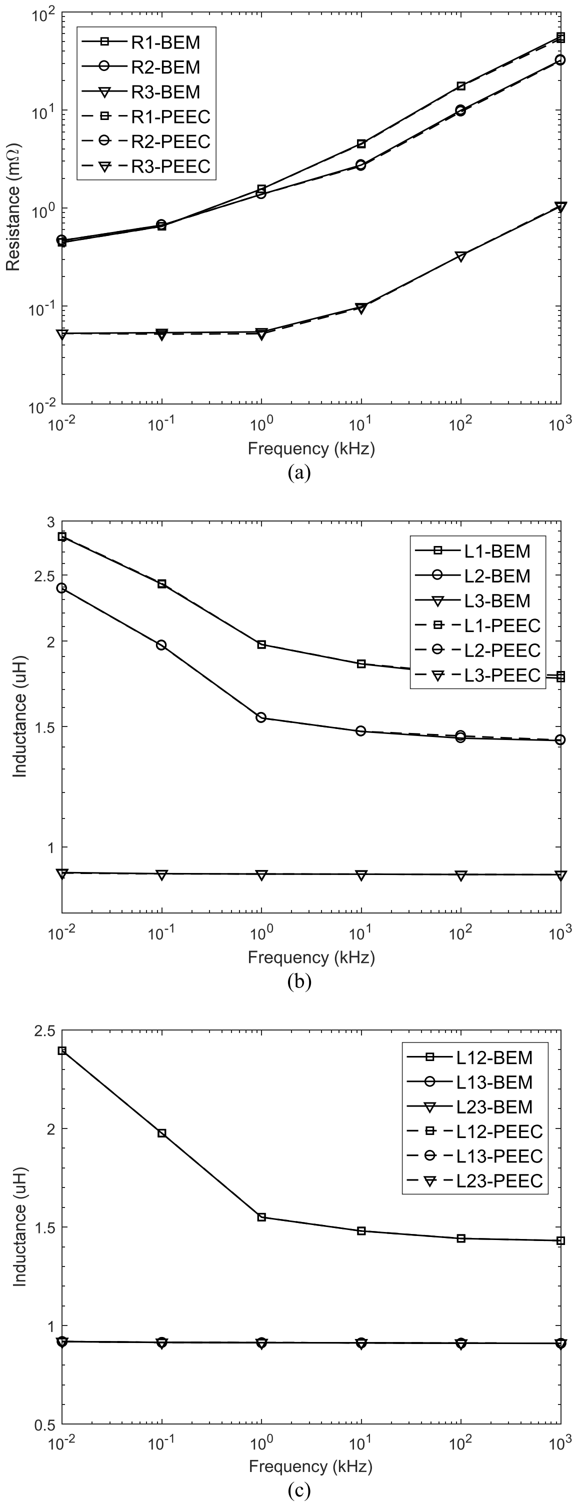


**FIGURE 7.** Comparison of (a) resistance, (b) self- inductance and (c) mutual inductance between commercial BEM and proposed PEEC method. (1, 2 and 3 corresponds to the index in Fig. 6).

to the equipment. While, cable sheaths are grounded to the earthing busbar ② in the other side of the room. The TS grounding grid is composed by a 3 m square tower mesh for the tower and a 9.5 m square mesh for the equipment

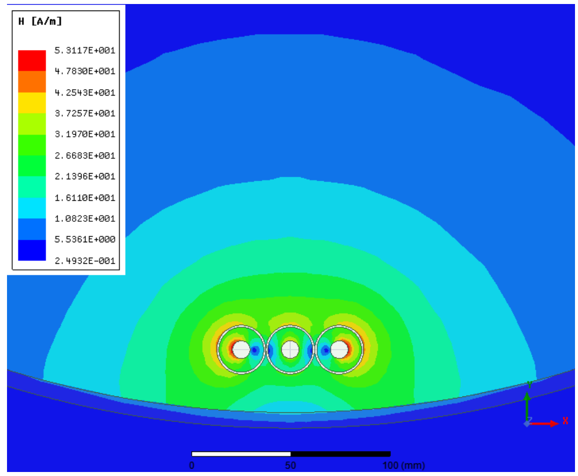


**FIGURE 8.** Magnetic field distribution on the cross section of the tubular tower with conductors at 10 kHz.

room as shown in Fig. 9(d). Two meshes are both buried at a depth of 0.7 m and are interconnected via three horizontal conductors. Besides the grid, eight 4 m long vertical electrodes are installed at the corners of grid meshes. The material and dimension information of conductors in TS are shown in Table 3.

**TABLE 3.** Information of conductors in TS.

| Material | $u_r$ | Conductivity (S/m) | W/Rout (mm) | T/Rin (mm) |
|---|---|---|---|---|
| Tower | 60 | $1.50\times10^6$ | - | - |
| Air-terminal | 42 | $1.50\times10^6$ | 20 | 0 |
| Grid | 42 | 0.27 | 40 | 4 |
| Electrode | 42 | 0.33 | 20 | 0 |
| COX | Sheath | $5.80\times10^7$ | 12.45 | 11.65 |
| | Core | $5.80\times10^7$ | 4.5 | 0 |
| SDC | Sheath | $3.78\times10^7$ | 4 | 3.4 |
| | Core | $5.80\times10^7$ | 1.3 | 0 |

In the simulation, the lightning strikes on the air-terminal of the system. The waveform of the lightning current is specified in IEC 62305 [28], and is defined by the Heidler's equation [29] as

$$i(t) = \frac{i_{\max}}{\eta} \frac{(t/T)^n}{1 + (t/T)^n} \exp(-t/\tau) \tag{10}$$

Lightning transient currents under the first and subsequent lightning stroke currents are investigated. The constants in (10) for these two waveforms are listed in Table 4.

Two soil resistivity, namely, 100 Ω·m and 1000 Ω·m representing low and high resistivity of the soil, are selected for comparison. The relative permittivity of soil is assumed to be 10. The grounding grid is modeled using the modified PEEC method with the reflection coefficient [18]. In the

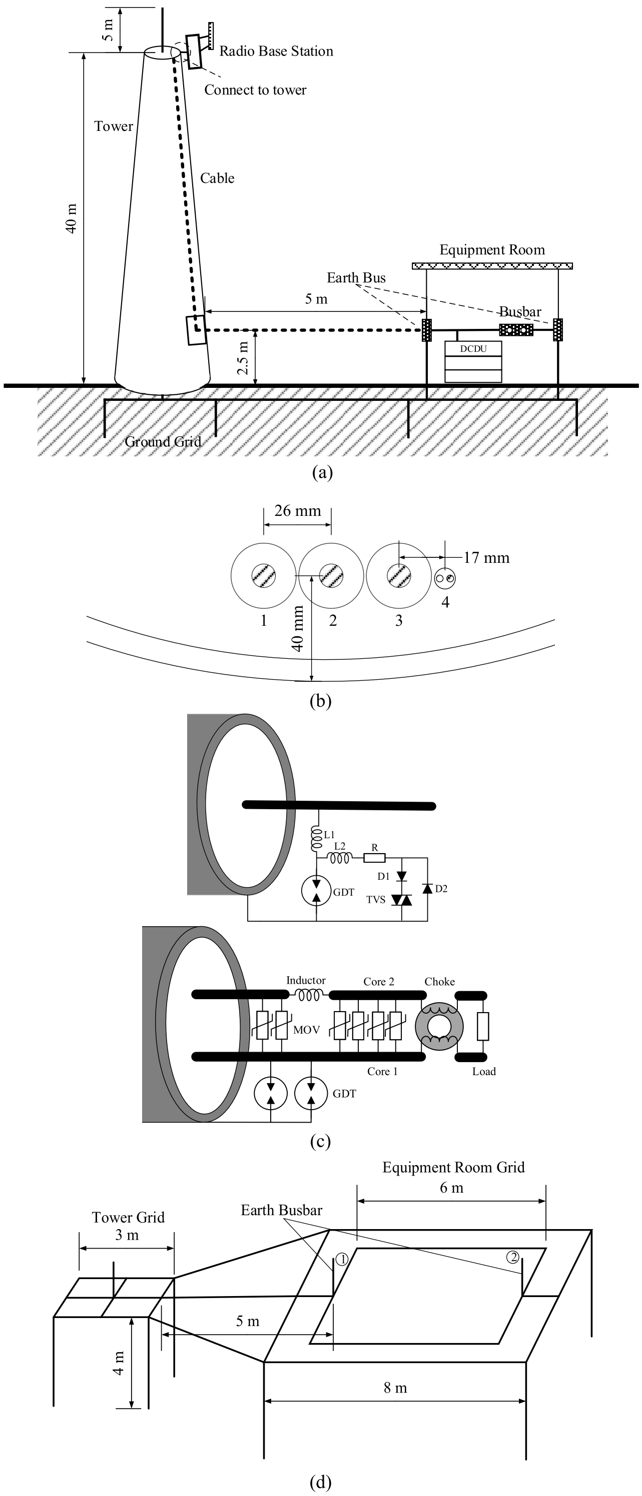


**FIGURE 9.** Schematic of a practical TS station with tubular tower. (a) Sideview of the TS with the equipment room. (b) Layout of the cables on cross section. (c) The lightning protection block for coaxial cable and SDC cable. (d) The schematic of the grounding meshes.

calculation, the grounding grid is segmented with the length of 5 m based on the wavelength in the soil. SPDs are modeled using the equivalent circuit models [17], [30].

**TABLE 4.** Parameters of the Two Heidler'S Functions.

| | $i_{max}$ (kA) | Waveform | $\eta$ | $T$ (μs) | $\tau$ (μs) |
|---|---|---|---|---|---|
| 1st Stroke | 100 | 1/200 | 0.986 | 1.82 | 285 |
| Sub. Stroke | 50 | 0.25/100 | 0.993 | 0.454 | 143 |

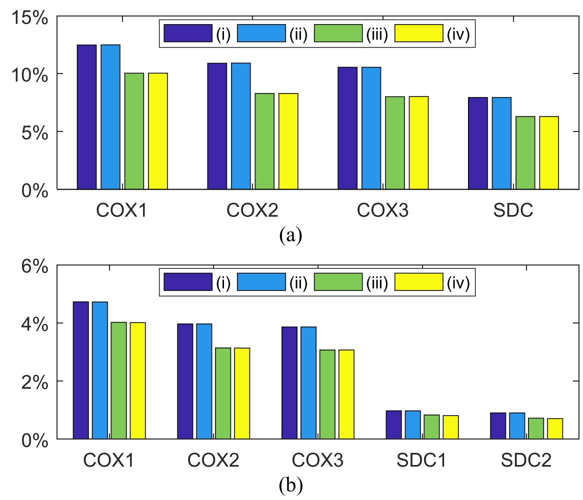


**FIGURE 10.** Normalized peak current distribution of studied cases. (a) Current distribution among cable sheaths. (b) Current distribution among cable cores. (The legend in figures indicate: (i) 1/200 $\mu$s waveform, Rsoil = 100 Ω·m; (ii) 1/200 $\mu$s waveform, Rsoil = 1000 Ω·m; (iii) 0.25/100 $\mu$s waveform, Rsoil = 100 Ω·m; (iv) 0.25/100 $\mu$s waveform, Rsoil = 1000 Ω·m.)

The simulation is conducted on HP Z840 Workstation with 2× Intel Xeon CPU E5-2650 2.3 GHz, 256 GB memory. The equivalent circuit parameters are calculated from 1 Hz to 1 MHz, which takes 28.7 min and 2.7 GB memory. The equivalent circuit of the system with SPDs is then evaluated in SPICE to 250 $\mu$s with time interval 0.1 $\mu$s in 4 min.

The lightning current is unevenly distributed among cables as the normalized peak current distribution in Fig. 10. Both first and subsequent current waveforms as well as low and high soil resistivity are considered for comparison. It is observed that the outmost cable (Cable 1) carries larger current than others due to the proximity effect. Meanwhile, by comparing the current distributions in the same cable with different soil resistivity, the resistivity of the soil shows negligible effects on the current distribution of the system.

The current distribution among cable sheaths, cables and the tower is shown in Fig. 11. It is noted that around 60% of the lightning current dissipates to the ground through the tower. 7% of the current dissipates at the earthing busbar ① through cable sheaths. While, the current flows through cable sheaths to the earthing busbar ② reaches about 25%, which is much greater than that in the earth bus ①. The current flows through cable cores also reach as high as 10%. This is probably caused by the "proximity" of the system that the current crowds or flows more in outer conductors. This

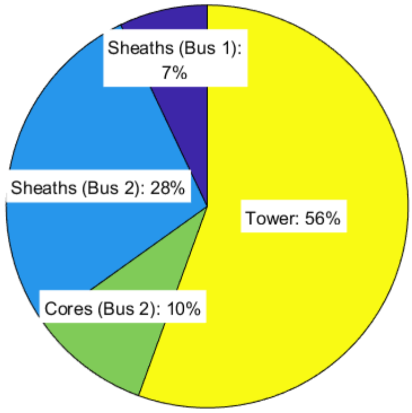


(a)

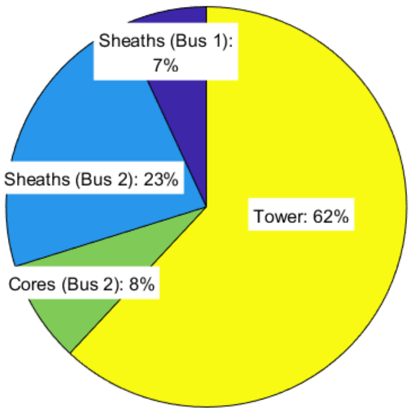


(b)

**FIGURE 11. Current distritution among cable sheaths, cores and the tower. (a) 1/200 $\mu$s waveform, Rsoil = 100 $\Omega$·m; (b) 0.25/100 $\mu$s waveform, Rsoil = 100 $\Omega$·m.**

phenomenon becomes more obvious under faster transients by comparing (a) and (b).

The current waveforms among cable sheaths, cable cores and the tower are presented in Fig. 12. For comparison, both the configurations with and without SPDs are investigated. In the configuration without SPD, all cable sheaths and cores are short connected representing the worst-case for current analysis. By comparing the currents with SPD (Fig. 12(a) and Fig. 12(b)) and without SPD (Fig. 12(c) and Fig. 12(d)), it is revealed that installed SPDs have little influence on the current distribution.

While, SPDs suppress high voltages between sheaths and cores of cables as shown in Fig. 13. The voltage between the sheath and the core of the coaxial cable 3 is constrained to 250 V for the first stroke (Fig. 13(a)) and 200 V for the subsequent stroke (Fig. 13(b)). It is suppressed to 100 V for the voltage between sheath and core 1 as well as that between two cores of SDC cable under these two lightning strokes. The open voltage is calculated for two types of lightning strokes as shown in Fig. 13(c) and Fig. 13(d). Open voltage represent the worst case for voltage analysis. In the open voltage calculation, the cable sheaths are also connected to the earthbus, while, the cable cores are unconnected. It is

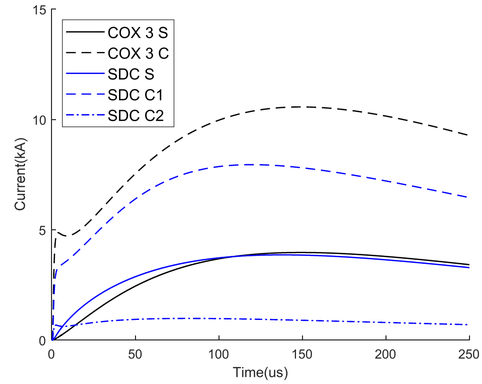


(a)

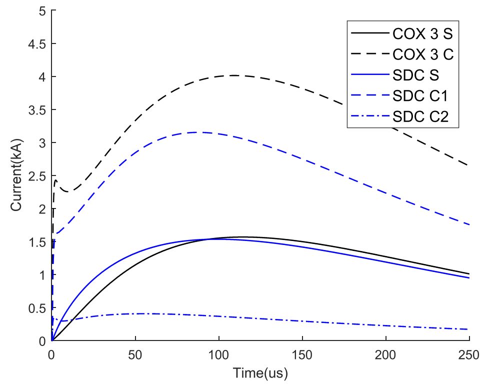


(b)

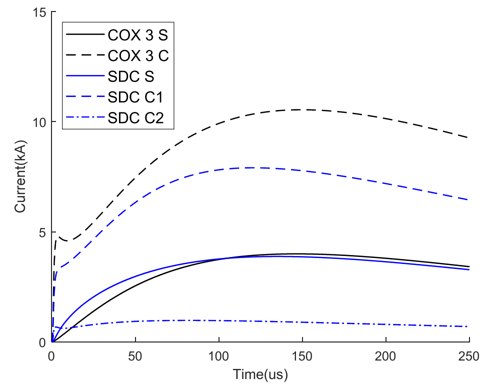


(c)

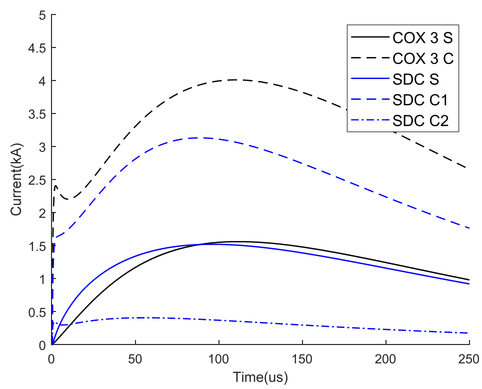


(d)

**FIGURE 12. Current waveform among cable sheaths, cores and the tower for the configuration with SPD: (a) 1/200 $\mu$s waveform, Rsoil = 100 $\Omega$·m; (b) 0.25/100 $\mu$s waveform, Rsoil = 100 $\Omega$·m, and without SPD: (c) 1/200 $\mu$s waveform, Rsoil = 100 $\Omega$·m; (d) 0.25/100 $\mu$s waveform, Rsoil = 100 $\Omega$·m.**

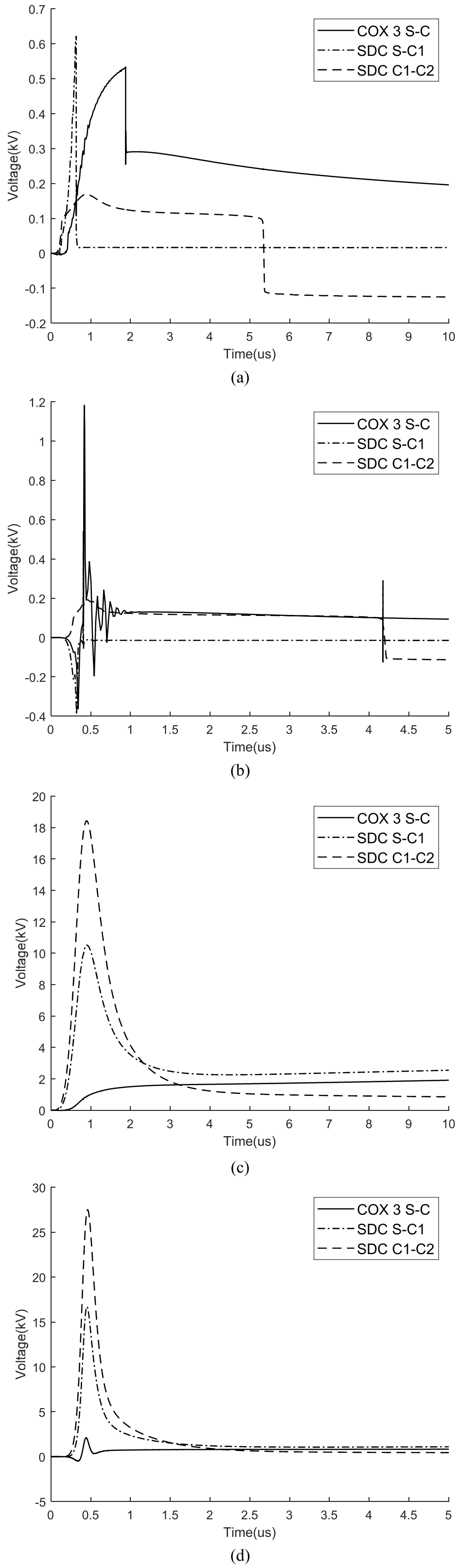


**FIGURE 13.** Voltage differences between sheaths and cores of cables for the configuration with SPD: (a) 1/200 $\mu$s waveform, Rsoil = 100 $\Omega$·m; (b) 0.25/100 $\mu$s waveform, Rsoil = 100 $\Omega$·m, and without SPD: (c) 1/200 $\mu$s waveform, Rsoil = 100 $\Omega$·m; (d) 0.25/100 $\mu$s waveform, Rsoil = 100 $\Omega$·m. (COX 1 S-C: between sheath and core of coaxial cable 1; SDC S-C1: between sheath and core 1 of SDC cable; SDC C1-C2: between two cores of SDC cable).

shown that the voltage difference between the cable sheath and the core can reach up to 20 kV when no SPD is installed. The voltage can be well suppressed to hundreds of volts when SPDs are installed.

## V. DISCCUSION AND LIMITATION OF PROPOSED METHOD

The proposed method has been implemented in the simulation tool TAES [31]. TAES is developed using Matlab as the calculation engine and has a C++ interface. It can be used to analyze the lightning transients in various systems with wire structures. While, it still has limitations.

The parameter matrix obtained using PEEC method is a dense matrix. The off-diagonal terms in the matrix (representing the mutual couplings) will lead to a long computation time for large systems. Therefore, model order reduction is required to further improve the efficiency of the proposed method in the future work.

Due to the retardation term is neglected, the proposed method is limited to simulate short conductors about dozens of meters long. For transmission lines of dozens of kilometers long, the retardation effect, ground effect, etc. should be considered, where the proposed method needs adjustment. The simulation tool will automatically classify different components and apply different methods in the future work.

The multi-layer ground is not supported in the current version of simulation tool. The dyadic Green's function (DGF) is the most accurate method for multilayer soil. While, DGF is solved in the frequency domain, which is hard to implement in the time domain. It is our future work to develop multi-layer ground model and implement it in the time domain using equivalent circuit.

## VI. CONCLUSION

A modeling procedure for a telecommunication system (TS) mounted on a tubular tower is presented in this paper. An efficient meshing scheme was proposed for modeling a system containing extremely large- and extremely small- radius conductors simultaneously. Both skin and proximity effects were accounted efficiently using the proposed method. The time-domain solution was performed using the extended equivalent circuit obtained by both partial element equivalent circuit (PEEC) method and Vector Fitting (VF) method. Numerical validation was presented in the paper as well. Finally, lightning current distribution in a practical TS was analyzed using the proposed approach. The following results are observed:

- The tubular tower has great influence on the current distribution of cables within it under direct lighting strikes though it is a Faraday cage.
- Lightning current among cables is unevenly distributed due to the proximity effect. More currents will distribute among the cables in the outer location.
- The surge protective devices for TS can suppress voltages to a safe level. While, they shows little influences on the current distribution.

- Current distribution is barely affected by the soil resistivity. Though, the soil with high resistivity could lead to large potentials in the system.
- Cables are connected to the earthing busbar both before and after entering the equipment room. A significant amount of the current dissipates in the busbar away from the lightning striking point.

## APPENDIX I
## INTEGRAL FORMULAS FOR INDUCTANCE OF UNALIGNED CONDUCTORS

For unaligned segments, semi-analytical formulas are adopted to calculate the mutual inductance. The tube tower can be assumed to be with zero thickness. Fig. 14 shows two general configurations of tower and cable segments.

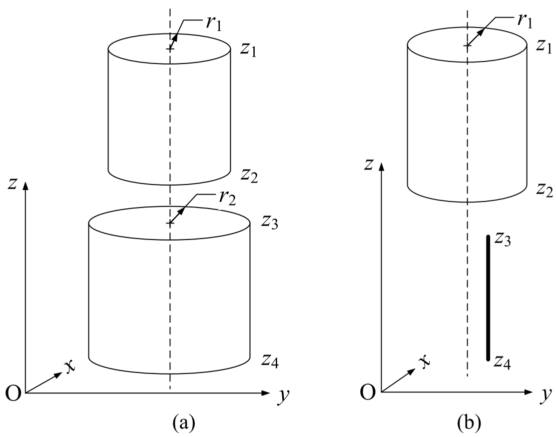


**FIGURE 14.** Schematic of unaligned condutors for integration. (a) Concentric cylinderical shells. (b) Cylinderical shell and filament.

The mutual inductance between different segments of the tubular tower as seen in Fig. 14(a) is calculated with the cylindrical shell integral. While, that between tower and cable segments as seen in Fig. 14(b) is calculated with the cylindrical-shell-filament integral. These two types of integrals have the kernel function as

$$F(z) = -T(z_{31}) + T(z_{32}) + T(z_{41}) - T(z_{42}) \tag{11}$$

in which $T(z_{ij}) = \ln\left(z_{ij} + \sqrt{z_{ij}^2 + A^2}\right) - \sqrt{z_{ij}^2 + A^2}$.

Cylindrical shell integral (Concentric) is obtained by

$$L_{ss}(z) = \frac{\mu_0}{4\pi}\frac{1}{K^2}\int_0^{2\pi} 2\pi r \cdot F(z)\, d\phi \tag{12}$$

where $A = \sqrt{r_1^2 + r_2^2 - 2r_1 r_2 \cos\phi}$ with $\phi = \alpha_1 - \alpha_2$, $K$ is the circumference of the shell cross section. Cylindrical-shell-filament integral is given by

$$L_{sf}(z) = \frac{\mu_0}{4\pi}\frac{1}{K}\int_0^{2\pi} r \cdot F(z)\, d\phi \tag{13}$$

where $A = \sqrt{r_1^2 + d^2 - 2r_1 d \cos\phi}$ with $\phi = \alpha_1$. Both integrals (12) and (13) can be obtained by integrating over $\theta$ from 1 to $2\pi$ using Gauss numerical integration.

## APPENDIX II
## INTEGRAL FORMULAS FOR INDUCTANCE OF ALIGNED CONDUCTORS

For parallel aligned cells with annular cross section, a formula for annular-cell-filament integral is derived in [12] and [22] to calculate the inductance using the point matching method.

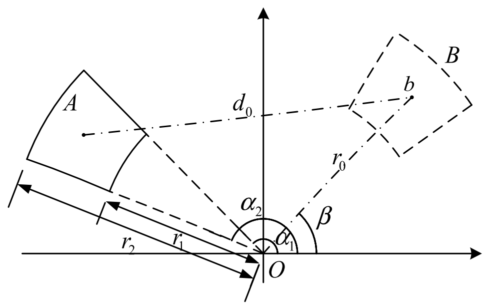


**FIGURE 15.** Schematic of annular-cell-filament cell (cross section view).

The schematic of the inductance cells is shown in Fig. 15, inductance between annular cell $A$ and cell $B$ is expressed by

$$\begin{aligned} L_{af} = \frac{\mu_0}{4\pi}\frac{1}{S}\int_{\alpha_1}^{\alpha} \Bigg\{ & r^2\left[l\ln(l + \sqrt{l^2 + d_0^2}) - \sqrt{l^2 + d_0^2} + d_0\right] \\ & + \frac{l}{2}\left(r^2 + 2rr_0\cos\theta\right) - l\left(r^2 - r_0^2\cos 2\theta\right)\ln d_0 \\ & + 2lr_0^2\sin\theta\cos\theta\arctan\frac{r - r_0\cos\theta}{r_0\sin\theta}\Bigg\} d\theta\Bigg|_{r_1}^{r_2} \end{aligned} \tag{14}$$

where $r_0$ is the distance between $O$ and the center of the field cell, $r_1$ and $r_2$ are the inner and outer radius of the source cell, and $S$ is the area of the annular section. Inductance is obtained by integrating over $\theta$ using the Gaussian quadrature rule.

## APPENDIX III
## INTEGRAL FORMULAS FOR CoP OF UNALIGNED CONDUCTORS

CoP between unaligned conductors can also be obtained using the cylindrical-shell-integral for segments of the tubular tower, and the cylindrical-shell-filament integral for tower and cable segments as shown in Fig. 14. Expressions of (12) and (13) can be used here with these coefficients, i.e.,

$$P_{ss}(z) = \frac{1}{4\pi\varepsilon_0}\frac{1}{l^2K^2}\int_0^{2\pi} 2\pi r \cdot F(z)\, d\phi \tag{15}$$

and

$$P_{sf}(z) = \frac{1}{4\pi\varepsilon_0}\frac{1}{l^2K}\int_0^{2\pi} r \cdot F(z)\, d\phi \tag{16}$$

## APPENDIX IV
## INTEGRAL FORMULAS FOR CoP OF ALIGNED CONDUCTORS

Similar to the inductance, the point-matching method is also adopted for CoP calculation. CoP for parallel aligned conductors is obtained using the arc-shell-filament integral.

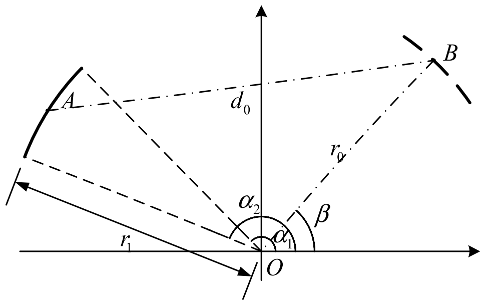


**FIGURE 16.** Schematic of arc-shell-filament cell (cross section view).

The schematic of the CoP cells is shown in Fig. 16, CoP between arc A and B can be approximated using the arc-shell-filament integral as expressed by

$$P_{af} = \frac{1}{4\pi\varepsilon_0}\frac{1}{l^2 K}\int_{\alpha_1}^{\alpha_2}\left\{2r_1\left[l\ln(l+\sqrt{l^2+d_0^2})-\sqrt{l^2+d_0^2}\right]\right.$$
$$\left. - l\ln R_{AB}^2 + 2\sqrt{R_{AB}^2}\right\}d\theta \qquad (17)$$

where $R_{AB} = \sqrt{r_1^2 + r_0^2 - 2r_1 r_0\cos(\theta-\beta)}$, $r_1$ is the radius of the source arc shell, $r_0$ is the distance form $O$ to the center of the field cell, and $K$ is the length of the arc. $P_{af}$ is obtained by integrating the last level $d\theta$ using Gaussian integration.

## REFERENCES

[1] L. Jike, Y. Qiangong, M. Xu, W. Zhigang, and Q. Zheng, "Statistics and analysis of lightning probability of radio base station," presented at the 30th Int. Conf. Lightning Protection (ICLP), 2010.

[2] T. Tominaga, N. Kuwabara, J. Kato, A. Ramli, A. Halim, and H. Ahmad, "Characteristics of lightning surges induced in telecommunication center in tropical area," *IEEE Trans. Electromagn. Compat.*, vol. 45, no. 1, pp. 82–91, Feb. 2003.

[3] C. F. Barbosa, F. E. Nallin, S. Person, and A. Zeddam, "Current distribution in a telecommunication tower struck by rocket-triggered lightning," presented at the 9th Int. Symp. Lightning Protection (IX SPIDA), Foz do Iguaçu, Brazi, 2007.

[4] C. Dai, Q. Wang, X. Zhang, S. Chen, and Z. Huang, "Lightning currents in DBS system from triggered-lightning experiments at Guangdong, China," in *Proc. Int. Conf. Lightning Protection (ICLP)*, 2014, pp. 131–135.

[5] T. Noda, A. Tatematsu, and S. Yokoyama, "Improvements of an FDTD-based surge simulation code and its application to the lightning overvoltage calculation of a transmission tower," *Electr. Power Syst. Res.*, vol. 77, no. 11, pp. 1495–1500, 2007.

[6] T. H. Thang, Y. Baba, V. A. Rakov, and A. Piantini, "FDTD computation of lightning-induced voltages on multiconductor lines with surge arresters and pole transformers," *IEEE Trans. Electromagn. Compat.*, vol. 57, no. 3, pp. 442–447, Jun. 2015.

[7] H. Chen, Y. Du, M. Yuan, and Q. H. Liu, "Lightning-induced voltages on a distribution line with surge arresters using a hybrid FDTD–SPICE method," *IEEE Trans. Power Del.*, vol. 33, no. 5, pp. 2354–2363, Oct. 2018.

[8] H. Chen, Y. Du, M. Yuan, and Q. H. Liu, "Analysis of the grounding for the substation under very fast transient using improved lossy thin-wire model for FDTD," *IEEE Trans. Electromagn. Compat.*, vol. 60, no. 6, pp. 1833–1841, Dec. 2018.

[9] G. Antonini, S. Cristina, and A. Orlandi, "PEEC modeling of lightning protection systems and coupling to coaxial cables," *IEEE Trans. Electromagn. Compat.*, vol. 40, no. 4, pp. 481–491, Nov. 1998.

[10] P. Yutthagowith, A. Ametani, N. Nagaoka, and Y. Baba, "Application of the partial element equivalent circuit method to analysis of transient potential rises in grounding systems," *IEEE Trans. Electromagn. Compat.*, vol. 53, no. 3, pp. 726–736, Aug. 2011.

[11] P. Yutthagowith, A. Ametani, F. Rachidi, N. Nagaoka, and Y. Baba, "Application of a partial element equivalent circuit method to lightning surge analyses," *Electr. Power Syst. Res.*, vol. 94, pp. 30–37, Jan. 2013.

[12] H. Chen and Y. Du, "Proximity effect modelling for cables of finite length using the hybrid partial element equivalent circuit and artificial neural network method," *IET Gener., Transmiss. Distrib.*, vol. 12, no. 16, pp. 3876–3882, 2018.

[13] H. Chen and Y. Du, "Model of ferromagnetic steels for lightning transient analysis," *IET Sci., Meas. Technol.*, vol. 12, no. 3, pp. 301–307, 2018.

[14] L. Grcev, A. P. J. V. Deursen, and J. B. M. V. Waes, "Lightning current distribution to ground at a power line tower carrying a radio base station," *IEEE Trans. Electromagn. Compat.*, vol. 47, no. 1, pp. 160–170, Feb. 2005.

[15] P. N. Mikropoulos, T. E. Tsovilis, and S. G. Koutoula, "Lightning performance of distribution transformer feeding GSM base station," *IEEE Trans. Power Del.*, vol. 29, no. 6, pp. 2570–2579, Dec. 2014.

[16] A. Tatematsu, K. Yamazaki, and H. Matsumoto, "Lightning surge analysis of a microwave relay station using the FDTD method," *IEEE Trans. Electromagn. Compat.*, vol. 57, no. 6, pp. 1616–1626, Dec. 2015.

[17] H. Chen, Y. Du, and M. Chen, "Lightning transient analysis of radio base stations," *IEEE Trans. Power Del.*, vol. 33, no. 5, pp. 2187–2197, Oct. 2018.

[18] H. Chen and Y. Du, "Lightning grounding grid model considering both the frequency-dependent behavior and ionization phenomenon," *IEEE Trans. Electromagn. Compat.*, to be published, doi: 10.1109/TEMC.2017.2789210.

[19] A. E. Ruehli, "Inductance calculations in a complex integrated circuit environment," *IBM J. Res. Develop.*, vol. 16, no. 5, pp. 470–481, 1972.

[20] C. R. Paul, *Introduction to Electromagnetic Compatibility*. Hoboken, NJ, USA: Wiley, 2006.

[21] H. Chen, Y. Du, and M. Chen, "Lightning current among closely-spaced cables," in *Proc. Int. Conf. Lightning Protection (ICLP)*, Shanghai, China, 2014, pp. 412–417.

[22] H. Chen and Y. Du, "Proximity effect in transient analysis of radio base stations," *Int. J. Numer. Model., Electron. Netw., Devices Fields*, p. e2335, 2018, doi: 10.1002/jnm.2335.

[23] S. Mei and Y. I. Ismail, "Modeling skin and proximity effects with reduced realizable RL circuits," *IEEE Trans. Very Large Scale Integr. (VLSI) Syst.*, vol. 12, no. 4, pp. 437–447, Apr. 2004.

[24] B. Gustavsen and A. Semlyen, "Rational approximation of frequency domain responses by vector fitting," *IEEE Trans. Power Del.*, vol. 14, no. 3, pp. 1052–1061, Jul. 1999.

[25] K. M. Coperich, J. Morsey, V. I. Okhmatovski, A. C. Cangellaris, and A. E. Ruehli, "Systematic development of transmission-line models for interconnects with frequency-dependent losses," *IEEE Trans. Microw. Theory Techn.*, vol. 49, no. 10, pp. 1677–1685, Oct. 2001.

[26] S. A. Schelkunoff, "The electromagnetic theory of coaxial transmission lines and cylindrical shields," *Bell Syst. Tech. J.*, vol. 13, no. 4, pp. 532–579, Oct. 1934.

[27] *Integrated Oersted*. Accessed: Oct. 2018. [Online]. Available: https://www.integratedsoft.com/Products/oersted.aspx

[28] *Protection Against Lightning—Part 1: General Principles*, Standard IEC 62305-1:2010, 2010.

[29] F. Heidler, J. M. Cvetic, and B. V. Stanic, "Calculation of lightning current parameters," *IEEE Trans. Power Del.*, vol. 14, no. 2, pp. 399–404, Apr. 1999.

[30] H. Chen and Y. Du, "A comprehensive study on the nonlinear behavior of metal oxide varistors," in *Proc. 33rd Int. Conf. Lightning Protection (ICLP)*, 2016, pp. 1–5.

[31] H. Chen, Z. Qin, Y. Du, Q. Wang, and Y. Ding, "TAES: A PEEC-based tool for transient simulation," in *Proc. Asia–Pacific Int. Symp. Electromagn. Compat. (APEMC)*, Shenzhen, China, 2016, pp. 676–678.

**HONGCAI CHEN** received the B.S. degree in electronic science from the Hefei University of Technology, Hefei, China, in 2012, and the Ph.D. degree in electrical engineering from The Hong Kong Polytechnic University, Hong Kong. From 2017 to 2017, he was a Visiting Scholar at Duke University, Durham, NC, USA.

He is currently a Research Assistant Professor with the SUSTech Academy for Advanced Interdisciplinary Studies, Southern University of Science and Technology, Shenzhen, China. His research interests are electromagnetic transient analysis, computational electromagnetics, model order reduction, and nonlinear system modeling.

**YANG ZHANG** received the B.S. degree in electrical engineering from the Huazhong University of Science and Technology, Wuhan, China, in 2011. He is currently pursuing the Ph.D. degree in electrical engineering with The Hong Kong Polytechnic University, Hong Kong.

His research interests are lightning protection, power system, and transformer diagnosis.

**YAPING DU** received the B.S. and M.S. degrees in electrical engineering from Shanghai Jiao Tong University, Shanghai, China, in 1984 and 1987, respectively, and the Ph.D. degree in electrical engineering from the University of Southern California, Los Angeles, CA, USA, in 1994.

He is currently a Professor with the Department of Building Services Engineering, The Hong Kong Polytechnic University. His research interests are electromagnetic environments, lightning protection, and power quality in electric power systems, and electrified railway systems and buildings.

Dr. Du is a member of the Institution of Electrical Engineers, and a Chartered Engineer of U.K.

**QINGSHA S. CHENG** received the B.Eng. and M.Eng. degrees from Chongqing University, Chongqing, China, in 1995 and 1998, respectively, and the Ph.D. degree from McMaster University, Hamilton, ON, Canada, in 2004.

In 1998, he joined the Department of Computer Science and Technology, Peking University, Beijing, China. In 1999, he joined the Department of Electrical and Computer Engineering, McMaster University, where was a Research Engineer.

He is currently an Assistant Professor with the Department of Electrical and Electric Engineering, Southern University of Science and Technology, Shenzhen, China. His research interests are surrogate modeling, CAD, modeling of microwave circuits, software design technology, and methodologies for microwave CAD.